

Theoretical investigation of tunable polarized broadband terahertz radiation from magnetized gas plasma

Xin-Yang Gu(顾新杨), Jin-Song Liu(刘劲松), Zhen-Gang Yang(杨振刚), Sheng-Lie Wang(汪盛烈), Ke-Jia Wang(王可嘉)
Citation: Chin. Phys. B . 2018, 27(5): 058701. **doi:** 10.1088/1674-1056/27/5/058701

Journal homepage: http://cpb.iphy.ac.cn; http://iopscience.iop.org/cpb

What follows is a list of articles you may be interested in

Ultra-compact terahertz switch with graphene ring resonators

Jian-Zhong Sun(孙建忠), Le Zhang(章乐), Fei Gao(高飞)
Chin. Phys. B . 2016, 25(10): 108701. **doi:** 10.1088/1674-1056/25/10/108701

Performance analysis of LDPC codes on OOK terahertz wireless channels

Chun Liu(刘纯), Chang Wang(王长), Jun-Cheng Cao(曹俊诚)
Chin. Phys. B . 2016, 25(2): 028702. **doi:** 10.1088/1674-1056/25/2/028702

Terahertz multi-metal-wire hybrid-cladding hollow waveguide for refractive index sensing

Ying-Ying Yu(于莹莹), Xu-You Li(李绪友), Kun-Peng He(何昆鹏), Bo Sun(孙波)
Chin. Phys. B . 2016, 25(2): 028703. **doi:** 10.1088/1674-1056/25/2/028703

Theoretical investigation on generating terahertz radiation from gas plasma induced by three-color ultrashort lasers

Wang Cheng-Liang, Yang Zhen-Gang, Liu Jin-Song, Wang Sheng-Lie, Wang Ke-Jia
Chin. Phys. B . 2015, 24(8): 088703. **doi:** 10.1088/1674-1056/24/8/088703

Design and optimization of terahertz directional coupler based on hybrid-cladding hollow waveguide with low confinement loss

Yu Ying-Ying, Li Xu-You, Sun Bo, He Kun-Peng
Chin. Phys. B . 2015, 24(6): 068702. **doi:** 10.1088/1674-1056/24/6/068702

Theoretical investigation of tunable polarized broadband terahertz radiation from magnetized gas plasma*

Xin-Yang Gu(顾新杨)[1], Jin-Song Liu(刘劲松)[1], Zhen-Gang Yang(杨振刚)[2], Sheng-Lie Wang(汪盛烈)[2], and Ke-Jia Wang(王可嘉)[1,†]

[1] *Wuhan National Laboratory for Optoelectronics, Huazhong University of Science and Technology, Wuhan* 430074, *China*
[2] *School of Optical and Electronic Information, Huazhong University of Science and Technology, Wuhan* 430074, *China*

(Received 16 November 2017; revised manuscript received 26 February 2018; published online 26 April 2018)

The mechanism of terahertz (THz) pulse generation with a static magnetic field imposed on a gas plasma is theoretically investigated. The investigation demonstrates that the static magnetic field alters the electron motion during the optical field ionization of gas, leading to a two-dimensional asymmetric acceleration process of the ionized electrons. Simulation results reveal that elliptically or circularly polarized broadband THz radiation can be generated with an external static magnetic field imposed along the propagation direction of the two-color laser. The polarization of the THz radiation can be tuned by the strength of the external static magnetic field.

Keywords: terahertz, plasma, magnetic field, polarization

PACS: 87.50.U–, 52.25.Jm, 52.38.Fz, 95.30.Gv **DOI:** 10.1088/1674-1056/27/5/058701

1. Introduction

In 1993, Hamster firstly observed sub-picosecond (ps) terahertz (THz) pulses from gas-plasma produced by single-color femtosecond (fs) laser.[1] Since then, more plasma-based THz generation schemes, such as external DC-bias, two-color fields and few-cycle pulses, have been reported.[2–4] Thanks to the development of laser pulses with higher power and shorter pulse-width, the THz peak electric field strength has exceeded few MV/cm and the bandwidth has reached up to 200 THz.[5,6] Thus gas plasma-based THz generation schemes are widely used in the laboratory today, and even commercial products have appeared.

Among these mentioned methods, the two-color experimental scheme, firstly reported by Cook *et al.* in 2000,[7] i.e., using a superposition of both fundamental and second-harmonic (SH) pulse fields to generate the plasma, has attracted the most research interest.[8–10] Its physical mechanism was initially treated as a four-wave mixing process. However, subsequent measured results overturned this intuitive explanation.[3,11] Using the so-called transient photocurrent model, Kim *et al.* pointed out that coherent THz waves originate from a net electron current surge generated by an asymmetric two-color laser field,[9,11] which is now widely accepted. Thus, based on this explanation, researchers have dedicated their efforts to finding various asymmetric ultrashort laser fields, in some cases with additional static electric or magnetic fields, to manipulate the emitted THz fields. For example, multiple-color fs-lasers can boost the THz conversion efficiency significantly to obtain higher intensity THz pulses.[12,13] Kim *et al.* demonstrated that the polarization of the THz wave is affected by successive polarization rotation of the local THz plasma sources and the velocity mismatch between the pump laser and the generated THz wave.[14] Appling a helical electric field along a plasma region, Lu *et al.* obtained an elliptically polarized THz wave.[15] Furthermore, the latest research suggests that polarization of the THz wave can be tuned by adjusting the time delays or intensity ratio in the input three-pulse configuration.[16] In 2015, Wang *et al.* reported that the magnetic plasma offers an approach to emit circularly or elliptically polarized THz radiation.[17] However, the results of their two-dimensional (2D) PIC simulations demonstrated that the generated circularly or elliptically polarized THz radiation is narrowband.

In this paper, we utilize the transient photocurrent (PC) model to theoretically investigate the mechanism of polarized THz pulse generation when a static magnetic field is imposed on the gas plasma along the propagation direction of the two-color laser. The simulation results demonstrate that the linearly polarized THz radiation under weak external B-field will be gradually turned to an elliptically or circularly polarized one when the magnetic field strength B is higher than 10 T. Moreover, the generated elliptically or circularly polarized THz wave is broadband rather than narrowband in Ref. [17], and its intensity can be enhanced. The physical mechanism is attributed to that the asymmetric acceleration process of the ionized electrons is changed from one-dimensional to two-dimensional due to the presence of the magnetic field.

It is noted that magnetic fields with tens of tesla, in the form of ms-pulsed field can be easily obtained.[18,19] Applying destructive methods, even hundreds of tesla, ns-

*Project supported by the National Natural Science Foundation of China (Grant Nos. 11574105, and 61475054) and the Fundamental Research Funds for the Central Universities, China (Grant No. 2017KFYXJJ029).

†Corresponding author. E-mail: wkjtode@sina.com

© 2018 Chinese Physical Society and IOP Publishing Ltd

pulsed and thousands of tesla, ns-pulsed B-fields are already available.[20–22] Compared with two-color fs-lasers and ps-THz pulses, these magnetic fields can be treated as static fields. Besides these traditional methods, Santos *et al.* proposed an enlightening method to generate kilo-tesla, ns-pulsed quasi-static B-fields by employing intense laser-driven capacitor-coil targets.[23,24] According to their reports, the B-field strength can be tuned by the laser energy and the B-field direction is perpendicular to the cross section of the hollow coil. By using this method, an all-optic scheme can be proposed that focuses the two-color laser on the coil center to generate a magnetized gas plasma.

2. Description of the physical process and PC models

As shown in Fig. 1, when two-color linearly polarized (along the x direction) fs-laser pulses are focused in a gas medium, a plasma will be generated around the focal point, where a static magnetic field is imposed on along the z-direction. Then the freed electrons form an asymmetric ionization current whose direction is deviated from the polarization direction of the fs-laser due to the Lorentz electromagnetic force.

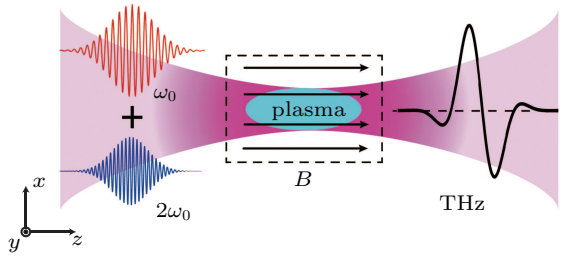


Fig. 1. (color online) Schematic diagram of THz generation in a photoinduced plasma using two-color laser with a static magnetic field imposed on the plasma.

Based on the PC model, the radiation field from plasma is proportional to the rate of change of such asymmetric ionization current, written as[9]

$$E_{\text{out}}(t) \propto \frac{\mathrm{d}J(t)}{\mathrm{d}t}, \tag{1}$$

where $J(t) = \int_{-\infty}^{t} -ev(t,t')\,\mathrm{d}N_{\text{e}}(t')$ is the ionization current. We use the static tunneling (ST) model to calculate electron density.[25] It is worth noting that the radiation from the plasma center contains many other frequency components. To extract the THz radiation field $E_{\text{T}}(t)$ from these frequency components, filtering and inverse Fourier transform $E_{\text{T}}(t) \propto \int_{-\infty}^{+\infty} f(\omega)\,\mathrm{d}\omega \int_{-\infty}^{+\infty} E_{\text{out}}(t')\,\mathrm{e}^{\mathrm{i}\omega t'}\,\mathrm{d}t'$ is used, in which $f(\omega)$ is a 100 THz low-pass filter function.

In our simulation, the fundamental laser has a Gaussian formation, center wavelength $\lambda = 800$ nm, full width at half maximum (FWHM) $T_{\text{FWHM}} = 50$ fs, and focal beam radius $w_0 = 10$ μm. According to the experimental scheme, a 0.1 mm thick type-I β barium borate (BBO) crystal is used to generate the second harmonic (SH) field. The peak intensities of the fundamental and the SH laser pulses after the BBO crystal are $I_\omega = 1.29 \times 10^{14}$ W/cm^2 and $I_{2\omega} = 0.45 \times 10^{14}$ W/cm^2, respectively. We assume that the fundamental and the SH laser pulses have the same polarization direction, which can be precisely controlled by a dual-band waveplate. The gas is nitrogen and its density is assumed to be 2.4×10^{19} cm^{-3}. The strength of the magnetic field $B \in [0, 1000\ \text{T}]$.

3. Results and discussion

Firstly, we obtain the THz E-field amplitudes along the x and y directions as the functions of time and magnetic field B, as depicted in Figs. 2(a) and 2(b), respectively. From these two figures, we extract some THz waveforms (E_x and E_y) corresponding to different B-values (see Figs. 2(c) and 2(d)). When $B < 10$ T, E_x is a single cycle pulse, while E_y has no significant value compared to E_x. Therefore, the B-field at this scale has little effect on the generation of THz radiation, which agrees with the conclusion in Ref. [17]. When B increases from 10 T to 500 T, the values of E_y are prominent and continually enhanced (see Fig. 2(d)), while the peak values of E_x are reduced gradually (see Fig. 2(c)). It is worth noting that both E_x and E_y are still single cycle pulses with the increase of B.

We plot the radiation spectra along two directions in the THz gap in Figs. 3(a) and 3(b) to investigate their characteristics. Figure 3(a) reveals that the B-field has no significant effect on the spectral range along the x direction, but induces a slight enhancement to the spectral amplitude. Figure 3(b) indicates that the spectrum along the y direction undergoes a process from scratch with increasing B. When $B = 10$ T, both spectral range and spectral amplitude along the y direction are much smaller than those along the x direction. With increasing B, the effective spectral range along the y direction is gradually enlarged. Three other different B-values (200 T, 350 T, and 500 T) correspond to the effective spectral ranges of 17 THz, 28 THz, and 40 THz, respectively. As a consequence, our simulations reveal that the THz radiation generated along both directions are broadband in this scheme and the effective spectral range along the y direction can be tuned by varying B.

Figures 3(c) and 3(d) plot the phase difference $\varphi_x - \varphi_y$ and the amplitude radio E_x/E_y between the x and y components in frequency domain with different B-field strengths, which are main characteristics of the polarized beams. When $B = 10$ T, the phase difference increases almost linearly with the frequency and the amplitude radio is greater than 1. Hence, the THz radiation is still nearly linearly polarized with $B = 10$ T. With increasing B, the curves of phase difference become smooth and gradually approximate the value of $-\pi/2$, see Fig. 3(c). In the meantime, the regions of the amplitude radio curves close to value 1 increase from several THz to tens of THz, as shown in Fig. 3(d). Summing up the above, the THz radiations change from linearly polarized to nearly broadband circularly polarized with the increase of B.

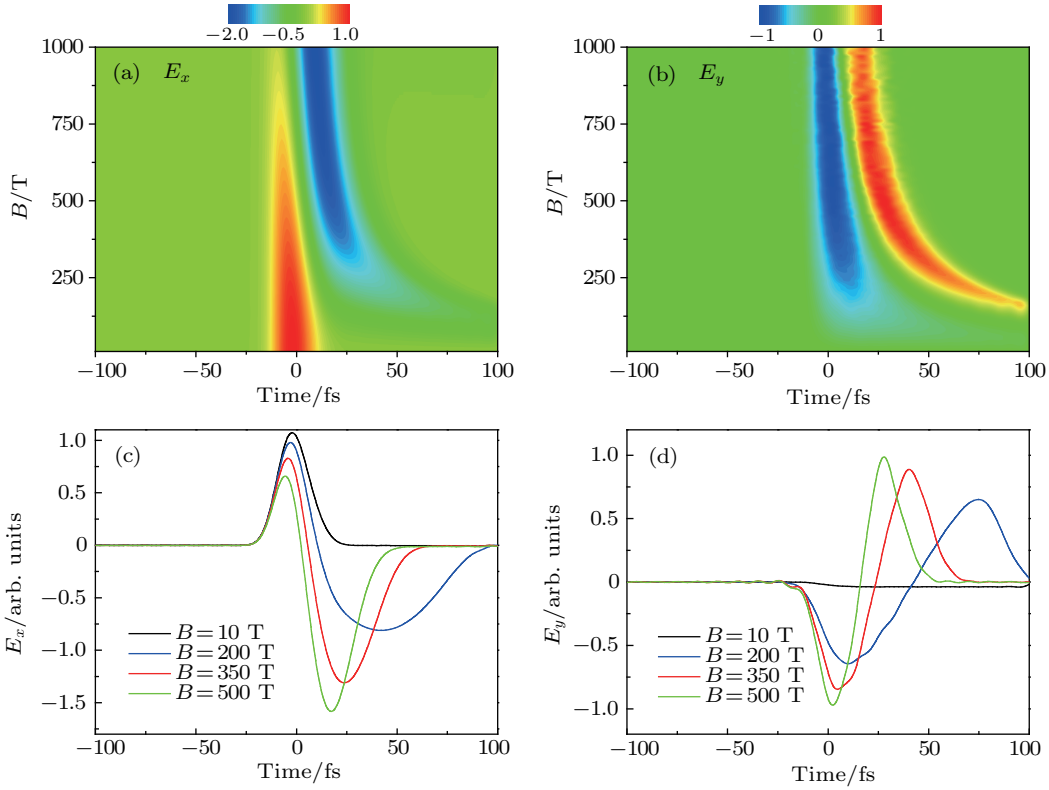


Fig. 2. (color online) (a) Calculated THz field amplitude along the x axis as a function of the time interval and the external magnetic field strength. (b) Calculated THz field amplitude along the y axis as a function of the time interval and the external magnetic field strength. (c) (d) Time-varying THz waveforms along the x and y axes in case of different magnetic field strengths.

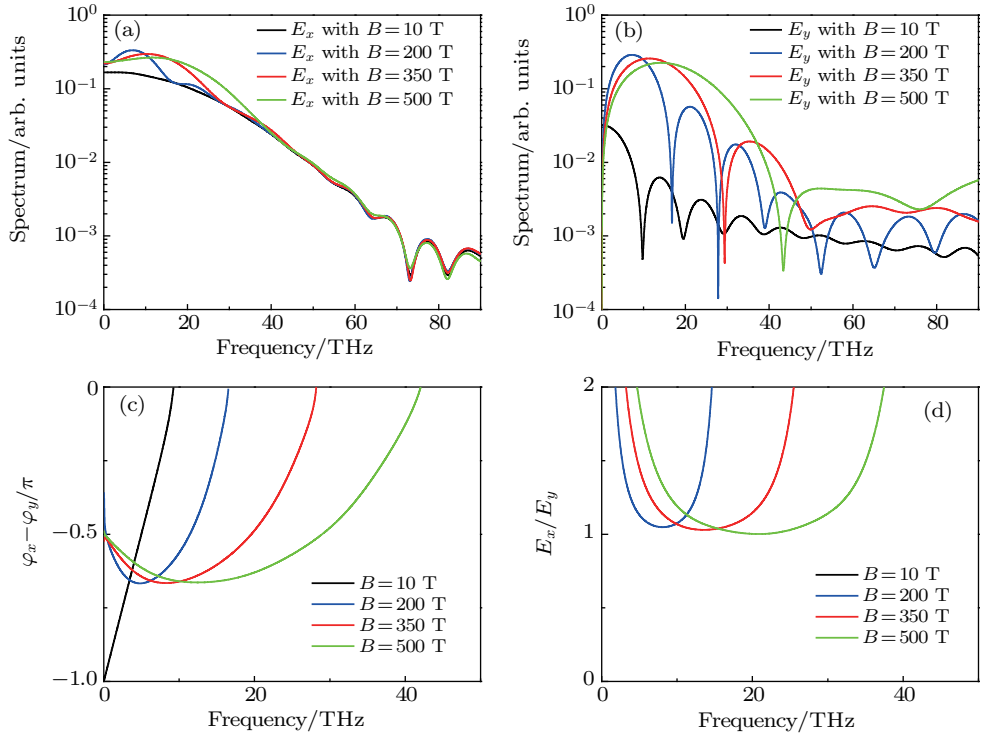


Fig. 3. (color online) (a) and (b) Radiation spectra along the x and y axes in case of different magnetic field strengths. (c) and (d) Phase difference and amplitude ratio between x and y components in frequency domain with different magnetic field strengths.

Next we plot the peak values of E_x and E_y versus B-field in Fig. 4(a). It is clear that the peak THz electric field along the x direction decreases consistently, while that along the y direction increases firstly and slightly decreases finally with increasing B. They become equal at 325 T. Figure 4(b) plots the THz pulse energy versus B, the maximum of the THz pulse energy is obtained at 410 T. Figure 4(c) plots the phase difference $\varphi_x - \varphi_y$ and the amplitude radio E_x/E_y between the x and

ycomponents in frequency domain with $B = 325$ T. We can find that the phase difference $\varphi_x - \varphi_y$ is around $-\pi/2$ for 0–20 THz and the amplitude radio E_x/E_y is approximately equal to 1 for 5–18 THz. Therefore, the THz radiation can be considered as a nearly broadband circularly polarized radiation when $B = 325$ T.

To further investigate the polarized properties of the THz radiation, we plot the three-dimensional THz electric field at $B = 325$ T and decompose it into three mutually orthogonal components with their polarization perpendicular to each other, as shown in Fig. 5(a). It is clearly seen that the absolute values of amplitude of the x and y components are almost equal. Thus the THz wave is approximate circularly polarized. Moreover, figures 5(b)–5(i) show the projections of the three-dimensional THz electric fields in the x–y plane, which make the relationship between the polarization of the THz radiation and the B-value more intuitive. The THz radiation is nearly linearly polarized when $B < 10$ T. With the increase of B, the linear polarization gradually turns into elliptically polarization. When B is up to 325 T, a nearly circularly polarized THz radiation is generated. Therefore, the polarization of the THz radiation is tunable via changing the B-field strength in this scheme.

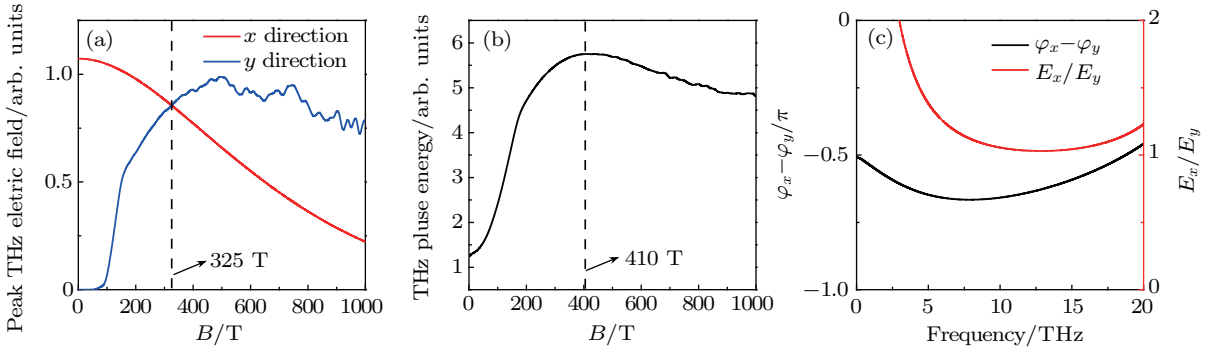


Fig. 4. (color online) (a) Peak THz electric fields along two directions versus the static magnetic field strength. (b) THz pulse energy versus the static magnetic field strength. (c) Phase difference and amplitude ratio between the x and y components in frequency domain when the magnetic field $B = 325$ T.

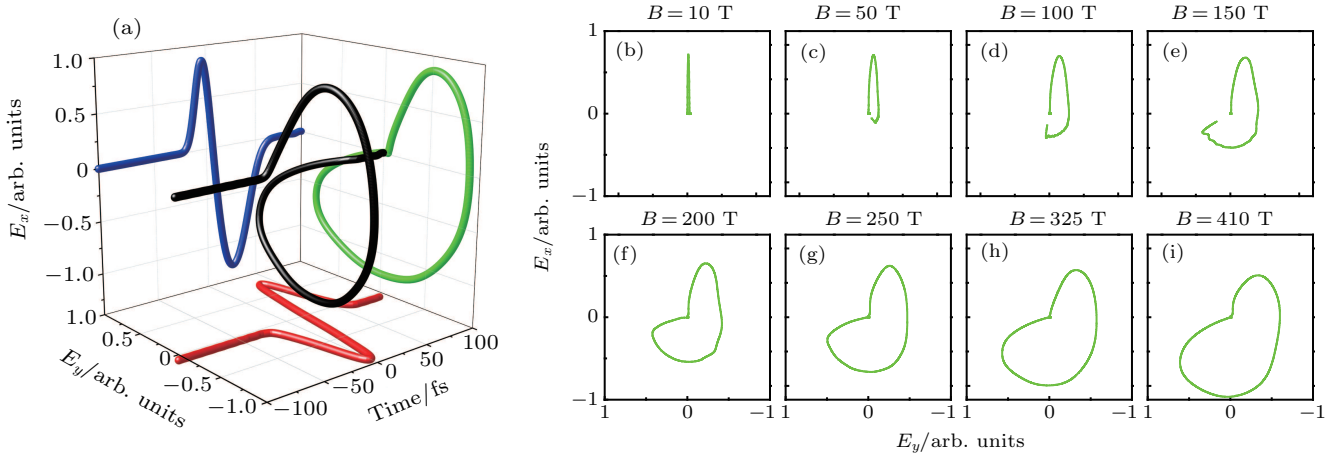


Fig. 5. (color online) (a) Temporal evolution of THz electric field with the magnetic field $B = 325$ T: three-dimensional (black) and projected (green) fields, as well as the x (blue) and y (red) components. (b)–(i) Projections of three-dimensional THz electric fields in x–y plane with different magnetic field strengths.

As mentioned above, the asymmetric ionization of bound electrons and the asymmetric electron acceleration play crucial roles in the whole process of THz generation. With an external B-field imposed on the gas plasma, these asymmetry processes could be more complex. By analyzing the force acting on the ionized electron motion, we will discuss our results. As the direction of the B-field is along the propagation direction of the two-color laser, the freed electrons will be deviated from the polarization direction of the laser due to the Lorentz force. After neglecting an attenuation item caused by the electron–ion collision, the freed electrons subjected to the laser field and static B-field accelerate as

$$\frac{\partial \boldsymbol{v}}{\partial t} = -\frac{e}{m}(\boldsymbol{E} + \boldsymbol{v} \times \boldsymbol{B}), \tag{2}$$

where e and m are the electron charge and mass, respectively. The electron velocities and forces in the x–y plane are plotted in Figs. 6(a) and 6(b). As the ionized electrons are driven by the asymmetric electric field and external B-field, the di-

rections of the electron velocity and Lorentz force will change constantly over time.

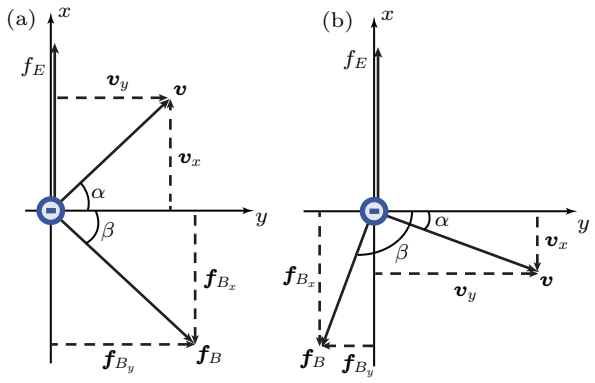


Fig. 6. (color online) (a) and (b) Electron velocity and forces in the x–y plane at different time.

We decompose the electron velocity and forces in the x and y directions at two different time, as shown in Figs. 6(a) and 6(b). Vectors $\boldsymbol{v}$ and $\boldsymbol{B}$ can be written as $\boldsymbol{v} = \boldsymbol{v}_x + \boldsymbol{v}_y = v_x\boldsymbol{e}_x + v_y\boldsymbol{e}_y$ and $\boldsymbol{B} = \boldsymbol{B}_x + \boldsymbol{B}_y = B_x\boldsymbol{e}_x + B_y\boldsymbol{e}_y$. Angle α is the angle between the velocity vector and the y axis. Angle β is the angle between the Lorentz force and the y axis, $\beta = \alpha - \pi/2$. No matter which quadrant velocity vector lies in, the acceleration of the electrons can be given by

$$\begin{cases} a_x = \dfrac{\mathrm{d}v_x}{\mathrm{d}t} = -\dfrac{e}{m}\left[E + |\boldsymbol{v}||\boldsymbol{B}|\sin\left(\alpha - \dfrac{\pi}{2}\right)\right], \\ a_y = \dfrac{\mathrm{d}v_y}{\mathrm{d}t} = -\dfrac{e}{m}\left[|\boldsymbol{v}||\boldsymbol{B}|\cos\left(\alpha - \dfrac{\pi}{2}\right)\right]. \end{cases} \tag{3}$$

By assuming that the initial electron velocity is zero ($v_{0,x} = v_{0,y} = 0$), the electrons are stationary and there is no Lorentz force at this time. The velocity of the electrons at the first discrete moment can be described by

$$\begin{cases} v_{1,x} = v_{0,x} + a_{0,x}\Delta t = eE(0)\Delta t/m, \\ v_{1,y} = v_{0,y} + a_{0,y}\Delta t = 0, \\ v_1 = v_{1,x}, \\ \alpha_1 = \pi/2, \end{cases} \tag{4}$$

where Δt is the discrete time step. Then the velocity of the electrons at the second discrete moment can be given by

$$\begin{cases} v_{2,x} = v_{1,x} + a_{1,x}\Delta t \\ \quad = v_{1,x} + e[E(1) + v_1|\boldsymbol{B}|\sin(\alpha_1 - \pi/2)]\Delta t/m \\ \quad = e\left[E\left(0\right) + E\left(1\right)\right]\Delta t/m, \\ v_{2,y} = v_{1,y} + a_{1,y}\Delta t = ev_1|\boldsymbol{B}|\cos(\alpha_1 - \pi/2)\Delta t/m \\ \quad = e^2|\boldsymbol{B}|E\left(0\right)\Delta t^2/m^2, \\ v_2 = \sqrt{v_{2,x}^2 + v_{2,y}^2}, \\ \alpha_2 = \arctan(v_{2,x}/v_{2,y}). \end{cases} \tag{5}$$

By applying the iterative method, the velocity of the electrons at the n-th discrete moment can be described by

$$\begin{cases} v_{n,x} = v_{n-1,x} + a_{n-1,x}\Delta t \\ \quad = v_{n-1,x} + e[E(n-1) \\ \quad\quad + v_{n-1}|\boldsymbol{B}|\sin(\alpha_{n-1} - \pi/2)]\Delta t/m, \\ v_{n,y} = v_{n-1,y} + a_{n-1,y}\Delta t \\ \quad = v_{n-1,y} + ev_{n-1}|\boldsymbol{B}|\cos(\alpha_{n-1} - \pi/2)\Delta t/m, \\ v_n = \sqrt{v_{n,x}^2 + v_{n,y}^2}, \\ \alpha_n = \arctan(v_{n,x}/v_{n,y}). \end{cases} \tag{6}$$

And so on, the velocity of the electrons at any discrete moment can be obtained. Substituting Eq. (6) into the following equation:

$$\begin{cases} L_{n,x} = L_{n-1,x} + v_{n-1,x}\Delta t, \\ L_{n,y} = L_{n-1,y} + v_{n-1,y}\Delta t, \end{cases} \tag{7}$$

we can obtain the electron displacements along two orthogonal directions at any discrete moment.

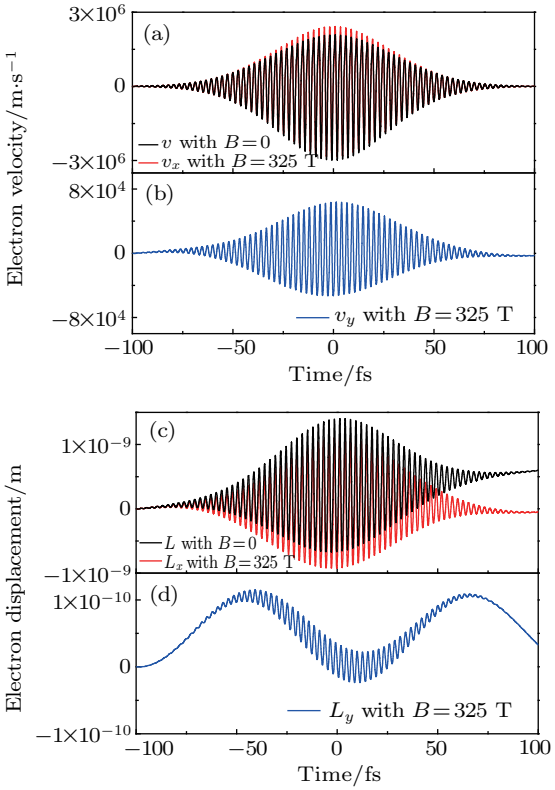


Fig. 7. (color online) (a) and (b) Electron velocities along two orthogonal directions with and without a static magnetic field. (c) and (d) Electron displacements along two orthogonal directions with and without a static magnetic field.

The electron velocities along the x and y directions are plotted in Figs. 7(a) and 7(b), from which it can be seen that an external B-field of 325 T introduces a y-component to the electron velocity, which complicates the electron motion in the two-dimensional space. In addition, figure 7(c) indicates that the ionized electrons only oscillate along the direction of the

laser polarization without a B-field. In contrast, with an external B-field of 325 T imposed, the electron motion turns to be two-dimensional, and the electron oscillation amplitude along the y direction is approximately one-tenth of that along the x direction, as shown in Figs. 7(c) and 7(d). As a result, the presence of the external B-field changes the ionized electron motion from one-dimensional to two-dimensional, generating elliptically or circularly polarized THz radiations.

4. Conclusion

By using the transient PC model, we systematically investigate the THz pulse generation when a static magnetic field is imposed on gas plasma along the propagation direction of the two-color laser. The influence of the static magnetic field is analyzed from the point of view of ionized electron motion. It is found that the static magnetic field introduces a y-component of electron motion, changing the THz radiation from the linearly polarized one to an elliptically or circularly polarized one. Our simulations demonstrate that the polarization of the THz radiation can be tuned by changing the magnetic field strength. If the magnetic field strength is less than 10 T, the THz radiation is still nearly linearly polarized. When the magnetic field strength increases, the generated THz radiation gradually turns to be elliptically or even nearly broadband circularly polarized. Consequently, this scheme offers an extremely significant way to obtain tunable polarized broadband THz radiation.

References

[1] Hamster H, Sullivan A, Gordon S, White W and Falcone R W 1993 *Phys. Rev. Lett.* **71** 2725

[2] Wang T J, Marceau C, Chen Y, Yuan S, Théberge F, Chateauneuf M, Dubois J and Chin S L 2010 *Appl. Phys. Lett.* **96** 211113

[3] Thomson M D, Kreß M, Löffler T and Roskos H G 2007 *Laser Photon. Rev.* **1** 349

[4] Dai J, Liu J and Zhang X C 2011 *IEEE J. Sel. Top. Quant. Electron.* **17** 183

[5] Oh T I, Yoo Y J, You Y S and Kim K Y 2014 *Appl. Phys. Lett.* **105** 041103

[6] Matsubara E, Nagai M and Ashida M 2012 *Appl. Phys. Lett.* **101** 011105

[7] Cook D J and Hochstrasser R M 2000 *Opt. Lett.* **25** 1210

[8] Clough B, Dai J and Zhang X C 2012 *Mater. Today* **15** 50

[9] Kim K Y, Taylor A J, Glownia J H and Rodriguez G 2008 *Nat. Photon.* **2** 605

[10] Andreeva V A, Kosareva O G, Panov N A, Shipilo D E, Solyankin P M, Esaulkov M N and Chin S L 2016 *Phys. Rev. Lett.* **116** 063902

[11] Kim K Y, Glownia J H, Taylor A J and Rodriguez G 2007 *Opt. Express* **15** 4577

[12] de Alaiza Martínez P G, Babushkin I, Bergé L, Skupin S, Cabrera-Granado E, Köhler C and Herrmann J 2015 *Phys. Rev. Lett.* **114** 183901

[13] Wang C L, Yang Z G, Liu J S, Wang S L and Wang K J 2015 *Chin. Phys. B* **24** 088703

[14] You Y, Oh T and Kim K Y 2013 *Opt. Lett.* **38** 1034

[15] Lu X and Zhang X C 2012 *Phys. Rev. Lett.* **108** 123903

[16] Wang H G, Li N, Bai Y, Liu P, Wang Z S and Liu C P 2017 *Opt. Express* **25** 30987

[17] Wang W M, Gibbon P, Sheng Z M and Li Y T 2015 *Phys. Rev. Lett.* **114** 253901

[18] Sims J, Baca A and Boebinger G 2000 *IEEE T. Appl. Supercon.* **10** 510

[19] Zherlitsyn S, Bianchi A D and Herrmannsdoerfer T 2006 *IEEE T. Appl. Supercon.* **16** 1660

[20] Singleton J, Mielke C H, Migliori A, Boebinger G S and Lacerda A H 2004 *Physica B* **346** 614

[21] Takeyama S and Kojima E 2011 *J. Phys. D: Appl. Phys.* **44** 425003

[22] Bykov A I, Dolotenko M I, Kolokolchikov N P, Selemir V D and Tatsenko O M 2001 *Physica B* **294** 574

[23] Santos J J, Bailly-Grandvaux M, Giuffrida L, *et al.* 2015 *New J. Phys.* **17** 083051

[24] Law K F F, Bailly-Grandvaux M, Morace A, Sakata S, Matsuo K, Kojima S, Lee S, Vaisseau X, Arikawa Y, Yogo A, Kondo K, Zhang Z, Bellei C, Santos J J, Fujioka S and Azechi H 2016 *Appl. Phys. Lett.* **108** 091104

[25] Corkum P B, Burnett N H and Brunel F 1989 *Phys. Rev. Lett.* **62** 1259